23rd ABCM International Congress of Mechanical Engineering
December 6-11, 2015, Rio de Janeiro, RJ, Brazil

PREDICTION OF NON-PROPORTIONAL STRAIN-HARDENING EFFECTS USING TANAKA'S POLARIZATION TENSOR ON 316 STAINLESS STEEL

Eleazar Cristian Mejia Sanchez
Marco Antonio Meggiolaro
Jaime Tupiassú Pinho de Castro
Pontificia Universidade Catolica do Rio de Janeiro, PUC-Rio
crisms@tecgraf.puc-rio.br
meggi@puc-rio.br
jtcastro@puc-rio.br

Abstract. *A tension-torsion machine (TTM) has been developed at PUC-Rio's Fatigue Laboratory to experimentally evaluate the non-proportional (NP) hardening behavior of materials subjected to multiaxial NP loadings. This machine independently applies over the test specimen tension/compression and torsion, which allows the generation of non-proportional multiaxial loading histories. To properly reproduce the stress-strain hysteresis loops in NP loading histories it is necessary to use incremental plasticity models. These models are based on three equations: the yield function, the plastic flow rule, and the hardening rule. An incremental plasticity simulator is developed for tension-torsion loads, incorporating the non-linear kinematic hardening model from Jiang-Sehitoglu, and the NP hardening model from Tanaka. The material parameters are calibrated using standard cyclic tests on uniaxial testing machines and tension-torsion tests on the developed TTM using 316-stainless steel cylindrical and tubular specimens. The simulations are able to predict the material behavior under different load histories, as well as different non-proportional hardening rates. The simulator performance is evaluated comparing the predicted and measured strain paths under the same input stress history. The simulations confirm the suitability of the incremental plasticity simulator implemented, based on the non-linear hardening models from Jiang-Sehitoglu and Tanaka.*

Keywords: *PID Sliding Control, Electromechanical Test Machine, Axial-Torsion Test Machine, Multiaxial Fatigue*

1. INTRODUCTION

Many engineering components are submitted to multiaxial stresses, in which the principal directions vary with time (Varvani-Farahani and Topper, 2000). Many practical applications such as in nuclear reactor vessels there are non-proportional stresses and strains under the combination of thermal and mechanical loadings. In specimen tests subjected to non-proportional stories, the phenomenon of NP hardening has an important role to predict the fatigue life. From the main works related to the study of non-proportional hardening models, one can mention those made by Sakane and Itoh (1999), which studied the microstructure of stainless steel 304 submitted to non-proportional strain paths (generated by tensile/torsion loading) at ambient temperature. In other work, Itoh (1999) studied the fatigue life in low cyclic of aluminum alloy 6061 subjected to 14 non-proportional strain paths (generated by tensile/torsion loading). The same author later studied the behavior of an alloy Ti-6Al-4V subjected to non-proportional loadings.

2. INCREMENTAL PLASTICITY

In most engineering applications, either the stress or the strain history is known, but not both. Generally, to design a new component, the stress history is calculated or estimated from measurements or specified design loads. In existing components, only the strain history can be measured, using strain gage rosettes. However, the best multiaxial fatigue damage models require the knowledge of both the stress and the corresponding strain histories to quantify the associated damage parameter. In the literature, several models correlate stress and strain for elastoplastic proportional stories, but to properly reproduce the stress-strain hysteresis loops in NP elastoplastic histories, which depend on the load path, it is necessary to use incremental plasticity models to correlate infinitesimal changes in all stress components with the associated strain components, and vice-versa.

2.1 Representation of stresses and strains in 5D space

A conventional way to represent incremental plasticity equations is to represent stress and strain tensors as 9-dimension column vectors $\bar{\sigma} = [\sigma_x \ \sigma_y \ \sigma_z \ \tau_{xy} \ \tau_{yx} \ \tau_{zx} \ \tau_{xz} \ \tau_{zy} \ \tau_{yz}]^T$ and $\bar{\varepsilon} = [\varepsilon_x \ \varepsilon_y \ \varepsilon_z \ \varepsilon_{xy} \ \varepsilon_{yx} \ \varepsilon_{zx} \ \varepsilon_{xz} \ \varepsilon_{zy} \ \varepsilon_{yz}]^T$, where $\tau_{ij} = \tau_{ji}$, $\varepsilon_{ij} = \varepsilon_{ji}$. The deviatoric stresses and strains are defined as the difference between stresses and strains and their hydrostatic components $\sigma_h = (\sigma_x + \sigma_y + \sigma_z)/3$ and $\varepsilon_h = (\varepsilon_x + \varepsilon_y + \varepsilon_z)/3$, which can be represented as $\overline{S} = [S_x\ S_y\ S_z\ \tau_{xy}\ \tau_{yx}\ \tau_{zx}\ \tau_{xz}\ \tau_{zy}\ \tau_{yz}]^T$ and $\overline{e} = [e_x\ e_y\ e_z\ \varepsilon_{xy}\ \varepsilon_{yx}\ \varepsilon_{zx}\ \varepsilon_{xz}\ \varepsilon_{zy}\ \varepsilon_{yz}]^T$, where $S_i = \sigma_i - \sigma_h$ and $e_i = \varepsilon_i - \varepsilon_h$. Other representations were proposed by Voigt and Mandel (1966), taking advantage of the symmetries $\tau_{ij}=\tau_{ji}$ and $\varepsilon_{ij}=\varepsilon_{ji}$ to express the stress or strain as 6-dimensional (6D) vectors. The deviatoric stresses S_x, S_y and S_z are linear-dependent, since $S_x + S_y + S_z = 0$, therefore it is possible to further reduce the dimension of deviatoric stresses from 6D to 5D, defining a 5D vector $\overline{S}' \equiv \overline{S}_{5D} = [S_1\ S_2\ S_3\ S_4\ S_5]^T$ (Bishop, 2000). The coordinate transformation from 6D space to 5D space involves a scaling factor k_s and a rotation angle ϕ_s as $\overline{S}'=A(k_s,\phi_s).\overline{\sigma}$ (Ilyushin,1961). The 5D Euclidean sub-space E_{5s} adopted in this work is similar to the one proposed by Papadopoulos, except that $k_s = 1$ to make its metric $|\overline{S}'|$ equal to σ_{Mises} (Papadopoulos, 1997).

$$\overline{S}'=\begin{bmatrix} S_1 \\ S_2 \\ S_3 \\ S_4 \\ S_5 \end{bmatrix} = \underbrace{\begin{bmatrix} 1 & -1/2 & -1/2 & 0 & 0 & 0 \\ 0 & \sqrt{3/2} & -\sqrt{3/2} & 0 & 0 & 0 \\ 0 & 0 & 0 & \sqrt{3/2} & 0 & 0 \\ 0 & 0 & 0 & 0 & \sqrt{3/2} & 0 \\ 0 & 0 & 0 & 0 & 0 & \sqrt{3/2} \end{bmatrix}}_{A} . \begin{bmatrix} \sigma_x \\ \sigma_y \\ \sigma_z \\ \tau_{xy}\sqrt{2} \\ \tau_{xz}\sqrt{2} \\ \tau_{yz}\sqrt{2} \end{bmatrix} \tag{1}$$

This 5D sub-space has several useful properties. The norm of a deviatoric stress is equal to the Mises equivalent stress $|S'|=\sigma_{\text{Mises}}$. Second, the distance between two stress states is equal to the von Mises stress range $\Delta\sigma_{\text{Mises}}$ between them. Finally, the locus of points that have the same $\Delta\sigma_{\text{Mises}}$ with respect to a point $\overline{S}'$ is a hypersphere with center in $\overline{S}'$ and radius $\Delta\sigma_{\text{Mises}}$. For load histories consisting of a combination of only uniaxial tension σ_x and torsion τ_{xy}, it is possible to represent their deviatoric components in a reduced-order 2D sub-space as

$$\overline{S}_{2D}=\begin{bmatrix} S_1 & S_3 \end{bmatrix}^T = [\sigma_x\ \ \tau_{xy}\sqrt{3}]^T \text{ and } \overline{e}_{2D}=\begin{bmatrix} e_1 & e_3 \end{bmatrix}^T = [\varepsilon_x.(1+\nu)\ \ \gamma_{xy}\sqrt{3}/2]^T \tag{2}$$

The Von Mises yield criterion in the 5D deviatoric space is given by

$$f = [(S_1\text{-}\beta_1)^2 + (S_2\text{-}\beta_2)^2 + (S_3\text{-}\beta_3)^2 + (S_4\text{-}\beta_4)^2 + (S_5\text{-}\beta_5)^2 - S^2] = |\overline{S}'\text{-}\overline{\beta}|^2 - S^2 = 0 \tag{3}$$

where S is the current yield strength, and $\overline{\beta}$ is the center of the yield surface, usually called backstress. The increment of plastic strain is given by the Prandtl-Reuss plastic flow rule as

$$d\overline{e}_p = (d\overline{S}'^T.\overline{n}').\overline{n}'/P \tag{4}$$

where P is the generalized plastic modulus, and $\overline{n}' = (\partial f/\partial\overline{S})/|f/\partial\overline{S}|$ is the normal vector in 5D perpendicular to the surface $f = 0$ at the current state $\overline{S}'$.

2.2 Incremental non-Proportional Hardening

Some materials subjected non-proportional (NP) multiaxial cyclic loads can lead to strain hardening much more than it would be expected from the uniaxial cyclic load. This phenomenon, called NP hardening, depends on the load history through the NP factor F_{NP} ($0 \le F_{NP} \le 1$), and the material through the additional hardening coefficient α_{NP} (where $0 \le \alpha_{NP} \le 1$) (Socie, 1999). The additional hardening coefficient α_{NP} is a parameter that reflects the material sensitivity to the non-proportionality of the loads. The NP hardening can be modelled by the uniaxial cyclic Ramberg-Osgood equation using a hardening coefficient H_{NP} and the cyclic exponent h_c, where

$$H_{NP} = H_c.(1+\alpha_{NP}.F_{NP}) \tag{5}$$

Figure 1 compares hysteresis loops produced by a NP out-of-phase tension-torsion history and a proportional history, both with the same normal strain amplitude $\Delta\varepsilon/2= 0.4$ % (Socie, 1999).

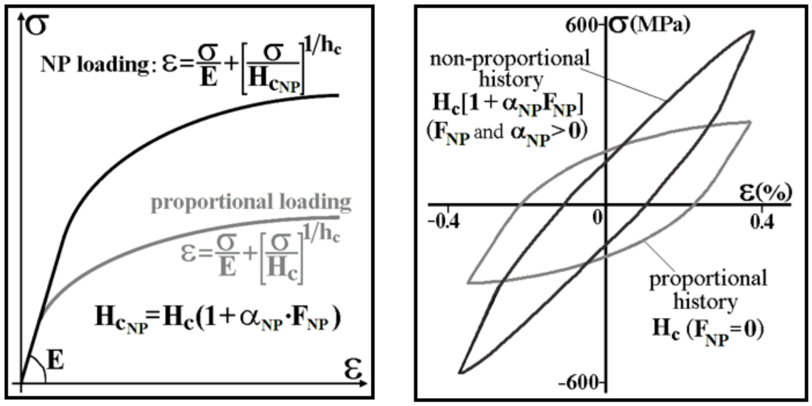

(a) (b)

Figure 1. a) Effect of NP cyclic loadings in NP hardening b) proportional and NP loops caused by same range of Δε in stainless steel 304 (Meggiolaro and Castro, 2009)

Tanaka's NP hardening model (Tanaka, 1994) makes use of a polarization tensor C_T that stores both the directionality and absolute value of the accumulated plastic strains through the eigenvalues and eigenvectors of C_T, respectively. The NP evolution of $F_{NP}(p)$ can be derived from the evolution of the yield surface radius S from a cyclically stabilized yield strength S_{Yc} to a target value as

$$\begin{aligned} S_{Yt} &= S_{Yc}.[1+\alpha_{NP}.(F_{NPt}+F_{NPm})] \\ dS &= (S_{Yt}-S).b_{NP}.dp \end{aligned} \tag{6}$$

where F_{NPt} is a target value of the NP factor, F_{NPm} is a memory factor that stores permanent hardening, b_{NP} is the NP hardening rate, and $dp = 2.|d\overline{e}_p'|/3$ is the equivalent plastic strain increment. The solution of the above evolution equation has the form

$$S = S_{Yc}.[1+\alpha_{NP}.F_{NP}(p)] \tag{7}$$

If equation (7) is replaced into (6), then

$$dS = [S_{Yc}.\alpha_{NP}.(F_{NPt}+F_{NPm}) - S_{Yc}.\alpha_{NP}.F_{NP}(p)].b_{NP}.dp \tag{8}$$

Finally, the evolution equation of the transient NP factor $F_{NP}(p)$ results in

$$dF_{NP}(p) = [F_{NPt}+F_{NPm}-F_{NP}(p)].b_{NP}.dp \tag{9}$$

In this work, the 90° out-of-phase experiments applied to the specimens result in $F_{NPt} = 1$, and the memory factor is not considered thus $F_{NPm} = 0$. In addition, using $S_y = H_m.(0.002)^{hc}$ and $S_{yc} = H_c.(0.002)^{hc}$, it is possible to obtain a transient Ramberg-Osgood coefficient evolution:

$$H(p) = H_c.[1+.\alpha_{NP}.F_{NP}(p)] \rightarrow \text{ NP evolution} \tag{10}$$

Using the plastic strain amplitude of each reversion in the Ramberg-Osgood equation, the evolution of $F_{NP}(p_i)$ and $F_{NP}(p_i)$ at each cycle *i* are given by

$$\begin{aligned} F_{NP}(p_i) &= [\alpha_{NP}.F_{NP}(p)]/\alpha_{NP} \\ H(p_i) &= H_c.\{1+[\alpha_{NP}.F_{NP}(p_i)]\} \end{aligned} \tag{11}$$

where b_{NP} is the NP hardening rate, F_{NP} is the NP factor, and α_{NP} is the additional hardening coefficient.

2.3 Surface translation rules

The rule adopted for the kinematic translation of these surfaces is the one proposed by (Jiang and Sehitoglu, 1996). The translation direction of each surface i is defined as,

$$\bar{v}_i' = \bar{n}'.\Delta S_i - (|\bar{\beta}_i'|/\Delta S_i)^{x_i}.\bar{\beta}_i' \tag{12}$$

where, x_i is a ratcheting exponent ($0 \leq x_i < \infty$). Then, the Generalized Plastic Modulus P is given by

$$P = (2/3).(p_1.\bar{v}_1'^T + p_2.\bar{v}_2'^T + ... + p_n.\bar{v}_n'^T).\bar{n}' = (2/3).(p.\bar{v}'^T).\bar{n}' \tag{13}$$

where p is an effective generalized plastic modulus coefficient (p_i are coefficients calibrated for each surface) and $\bar{v}'$ is an effective translation direction.

3. EXPERIMENTAL SYSTEM

The tension-torsion machine (TTM), developed at PUC-Rio's Fatigue Laboratory, was used to evaluate the NP hardening model experimentally. This electromechanical system created for multiaxial fatigue testing consists of an arrangement of individual and interconnected components to provide traction and/or torsion on the test specimen. The TTM was designed to work with a maximum capacity of 25 kN in traction and 1300 N.m in torsion, which is able to produce the same effects on the specimen test in pure tension or pure torsion. Figure 4 shows the TTM machine.

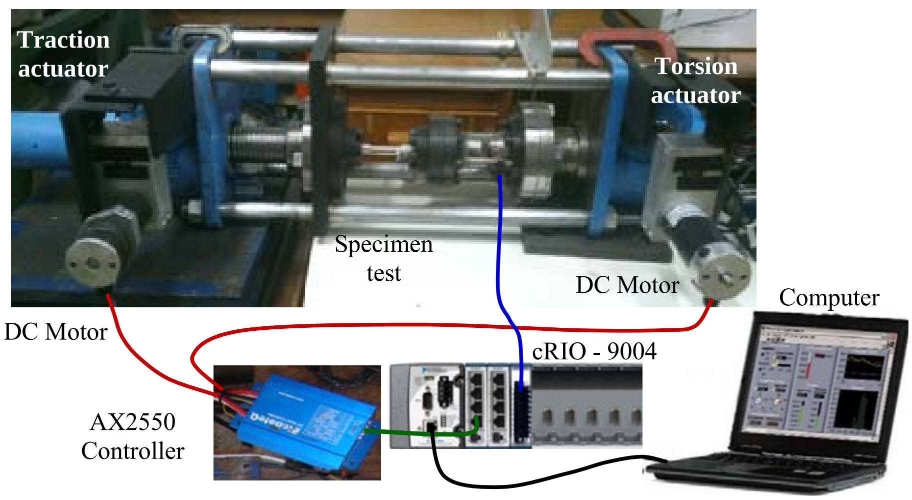

Figure 4. The TTM developed at PUC-Rio's Fatigue Laboratory

The TTM is composed of two mechanical actuators, load transmission elements, transducers to measure the variable to be controlled, a control system provided with user-machine interface, and its mechanical structure as shown in figure 4. The electric connections of the TTM are constituted by two parts. First, data reading that includes the connection of load torque cell and LVDT's to NI-9237 data acquisition module of the CompactRio, a module provided by National Instruments; and second, the control system connection that includes the connection of cRIO NI-9263 to an AX2550 controller, which controls each TTM actuator (a DC motor) through proportional control. The TTM control system was developed using the compactRIO CRio-9004, using LabVIEW 9.0 to perform the tests on the experimental system described above, which includes acting on the system and reading data. The user can visualize the errors in real time, paths of the desired loads, paths of axial force and torque, paths of normal and shear stress, as well as position and rotation values.

4. SIMULATION AND EXPERIMENTAL RESULTS

The NP hardening for stainless steel 316 was evaluated experimentally using the TTM machine. The cyclic hardening parameters of the material required by the simulator were obtained from experiments on an INSTRON-8501 test machine. Afterwards, the experimental strain path measured in the TTM was compared with the one predicted by the NP hardening model simulator. In the NP hardening testing, a tubular test specimen is used, with outer diameter $\phi_e = 14,9$, inner diameter $\phi_1 = 12.8$ and length $L_c = 140$ mm, subjected to a cyclic tension-torsion 90° out-of-phase load. The cyclic hardening parameters H_c and h_c of the Ramberg-Osgood equation for 316 stainless steel were obtained by the linear fitting of the points at the peaks (Δσ/2, Δε/2) of the strain hysteresis loop in log-log (see figure 5).

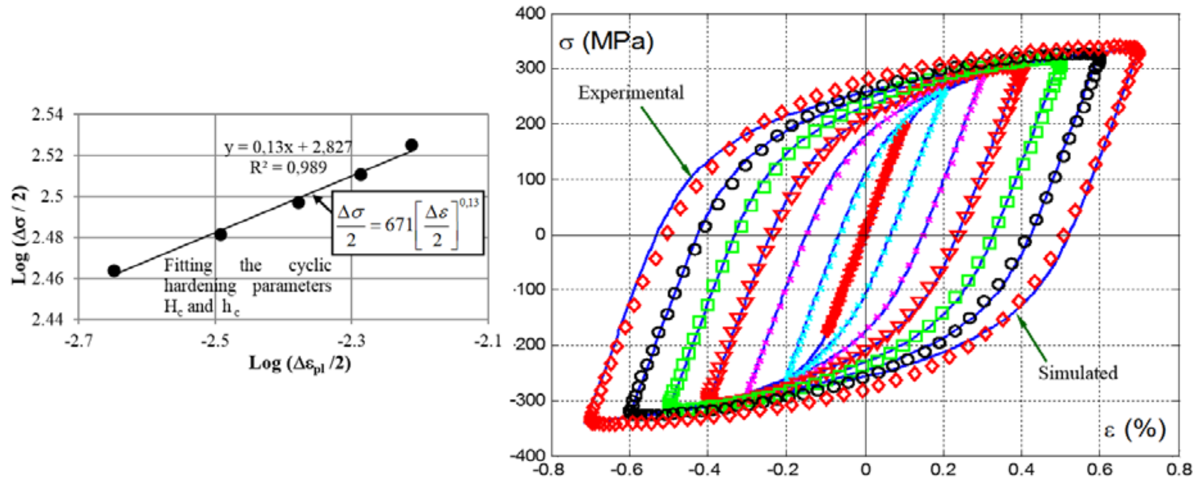

(a) (b)

Figure 5. a) Fitting of the cyclic hardening parameters and b) hysteresis loops of the stainless steel 316.

The NP hardening tests consist of subjecting the tubular specimen test to a desired tension $\sigma(t) = \sigma_a.\sin(\omega t)$ and a desired 90° out-of-phase torsion $\tau(t) = \tau_a.\cos(\omega t)$ in load and torque control, respectively, where $\tau_a = \sigma_a.\sqrt{3}$. During the test, the strains ε_x, ε_y, γ_{xy} of the tubular specimen were measured using an image correlation module (VIC-3D - Correlated Solutions). The shear stress was determined from the normal stress, defined as the stress that produces the same von Mises stress under pure tension. In the first test, an axial stress $\sigma_x(t) = 200.\sin(\omega t)$ MPa was chosen, able to generate an axial strain $\varepsilon_x = 0.1\%$, and a 90º out-of-phase shear stress $\tau(t) = 115.\cos(\omega t)$ MPa was chosen, generating a NP loading on the test specimen.

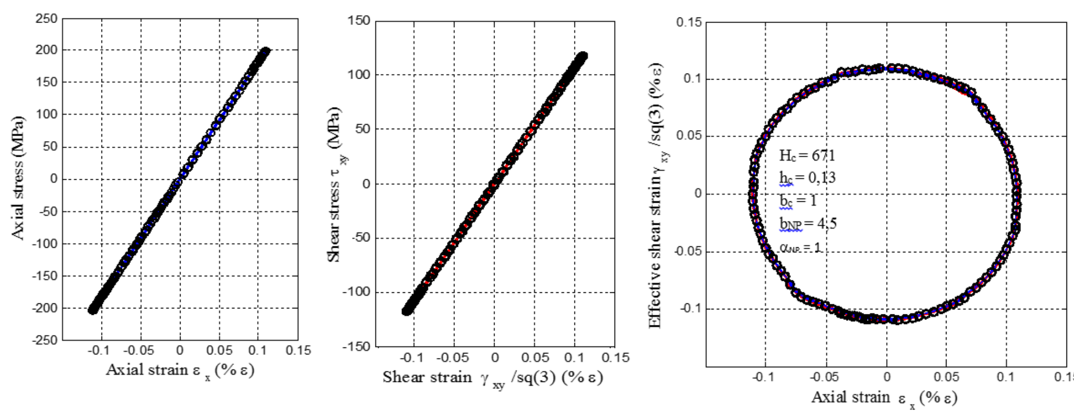

(a) (b) (c)

Figure 6. NP hardening test: a) hysteresis loop σ_x-ε_x; b) hysteresis loop τ_x-γ_{xy}; and c) strain path ε_x-$\gamma_{xy}/\sqrt{3}$.

The NP load chosen for the first test did not generate NP hardening in the material. In a second test, the tubular specimen test was subjected to an axial stress $\sigma_x(t) = 300.\sin(\omega t)$ MPa, generating an axial strain $\varepsilon_x = 0.25\%$, and with 90º out-of-phase shear stresses $\tau(t) = 173.\cos(\omega t)$ MPa. The test results are presented in figure 7.

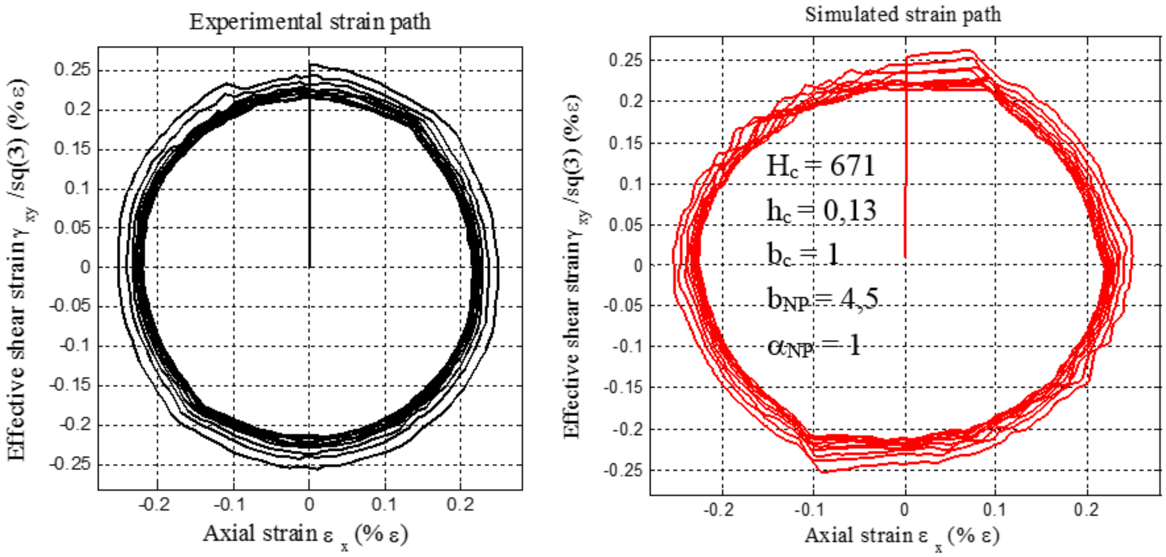

a) b)

Figure 7. NP hardening test: a) experimental strain path ε_x-$\gamma_{xy}/\sqrt{3}$; b) simulated strain path ε_x-$\gamma_{xy}/\sqrt{3}$.

In the third test, the tubular specimen was subjected to an axial stress $\sigma_x(t) = 342.\sin(\omega t)$ MPa, generating an axial strain $\varepsilon_x = 0.31\%$, and 90º out-of-phase shear stress $\tau(t) = 200.\cos(\omega t)$ MPa. The test results are presented below.

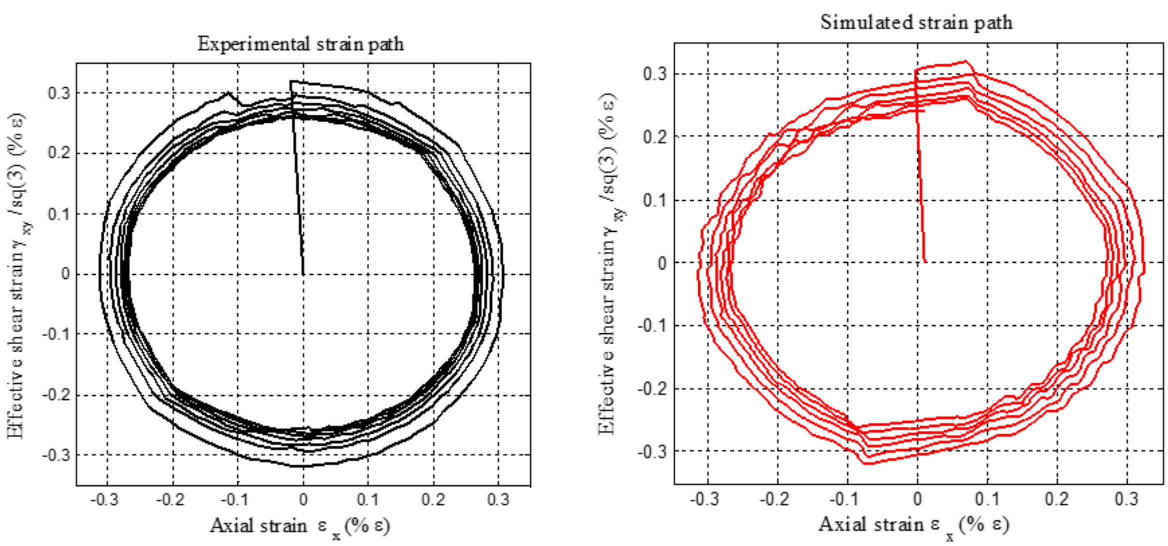

a) b)

Figure 8. Testing of NP hardening a) experimental strain path ε_x-$\gamma_{xy}/\sqrt{3}$ b) simulated strain path ε_x-$\gamma_{xy}/\sqrt{3}$.

Figures 7.a and 8.a show that the strain path begins with a larger radius, which decreases for each cycle due to NP hardening. The experimental strain path shows the same behavior as the simulated one.

Figure 9 shows the strain path obtained for each NP hardening test. In the first test, the material didn't show NP hardening, because the stress state in the material remained in the elastic zone, however in the second (2) and third (3) tests it exhibits significant strain hardening,

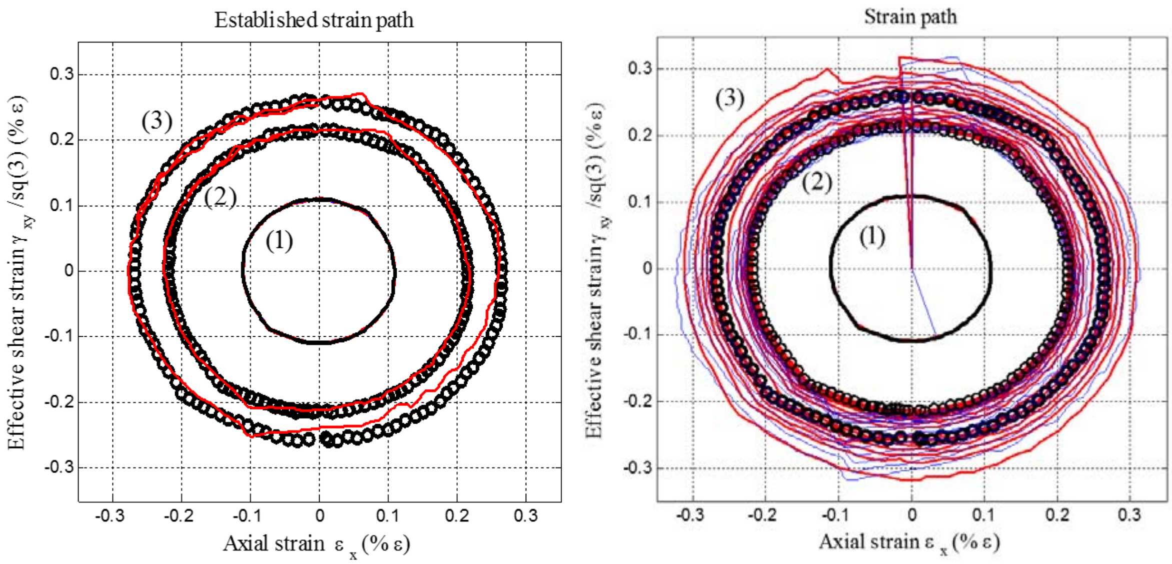

Figure 9. a) Imposed strain path; b) Strain path ε_x -$\gamma_{xy}/\sqrt{3}$ in NP hardening tests of stainless steel 316 with ε_x=0,1%, ε_x=0,25% and ε_x=0,31%.

5. CONCLUSIONS

In this work, it was verified that the 5D representation of deviatoric stresses and strains is highly recommended, since it reduces the dimensionality of the stress-strain relations from 6D to 5D, decreasing computational cost in incremental plasticity simulations. Moreover, for specimen tests without notches subjected to tension-torsion NP histories or uniaxial loading, it would be possible to use a 2D or 1D subspace of the 5D representation, respectively, further reducing computational cost. Experiments on 316 stainless steel showed that the implemented incremental plasticity simulation routines are able to predict the significant NP hardening effect.

6. REFERENCES

Bishop, J.E., 2000. Characterizing the non-proportional and out-of-phase extend of tensor paths, Fatigue and Fracture of Engineering Materials and Structures, v.23, pp.1019-1032.

Ilyushin, A.A., 1961, On the foundations of the general mathematical theory of plasticity. In: Voprosy Teorii Plastichnosti, pp. 3-29. Moskva: Izd. AN SSSR. (In Russian.)

Jiang, Y., Sehitoglu, H., 1996. “Modeling of Cyclic Ratchetting Plasticity, Part I: Development of Constitutive Relations,” ASME Journal of Applied Mechanics, v.63, n.3, p.720-725.

Jiang, Y., Sehitoglu, H., 1996. “Modeling of Cyclic Ratchetting Plasticity, Part II: Comparison of Model Simulations with Experiments” ASME Journal of Applied Mechanics, v.63, n.3, p.726-733.

Mandel, J., 1966. Cours de Mécanique des Milieux Continus, tomes I and II, Gauthier-Villars, Paris.

Meggiolaro, M.A., Castro, J.T.P, 2009. Tecnicas practicas de Dimensionamiento estrutural sobre reais em serviço – Vol I, Rio de Janeiro, CreateSpace, pp. 423-426.

Mróz, Z., 1967. "On the description of anisotropic workhardening", Journal of the Mechanics and Physics of Solids, v.15, n.3, p.163-175.

Papadopoulos IV, Davoli P, Gorla C, Filippini M, Bernasconi A, 1997. A comparative study of multiaxial high-cycle fatigue criteria for metals. Int J Fatigue; 19:219–35. (Reduced Euclidean space, good review of Mohr-type criteria)

Socie, D.F., Marquis, G.B., 1999. Multiaxial Fatigue, SAE.

Tanaka, E., 1994. A non-proportionality parameter and a cyclic viscoplastic constitutive model taking into account amplitude dependences and memory effects of isotropic hardening, European Journal of Mechanics - A/Solids, v.13, p.155–173.

7. RESPONSIBILITY NOTICE

The authors are the only responsible for the printed material included in this paper.